

**PHOTOMETRIC REDSHIFTS OF GALAXIES IN THE HUBBLE DEEP
FIELD**

KENNETH M. LANZETTA, ALBERTO FERNÁNDEZ-SOTO¹, and AMOS YAHIL
Department of Physics and Astronomy, State University of New York at Stony Brook
Stony Brook, NY 11794–3800, U.S.A.

arXiv:astro-ph/9709166v1 17 Sep 1997

¹Current address: School of Physics, University of New South Wales, P.O. Box 1, Kensington, NSW 2033,
AUSTRALIA

ABSTRACT

We describe our application of broad-band photometric redshift techniques to faint galaxies in the Hubble Deep Field. To magnitudes $AB(8140) < 26$, the accuracy of the photometric redshifts is a few tenths and the reliability of the photometric redshifts approaches 100%. At fainter magnitudes the effects of photometric error on the photometric redshifts can be rigorously quantified and accounted for. We argue that broad-band photometric redshift techniques can be applied to accurately and reliably estimate redshifts of galaxies that are up to many magnitudes fainter than the spectroscopic limit.

1. INTRODUCTION

Between 2500 and 3500 objects (depending on exactly how they are counted) are visible in the Hubble Deep Field (HDF) images obtained by the Hubble Space Telescope (HST), to a limiting magnitude threshold that approaches $AB(8140) \approx 30$. Spectroscopic redshift identifications of just over 100 of these objects—or roughly 3% of the total—have been obtained with the Keck telescope, following nearly two years of intensive effort. The faintest objects that have been (or presumably can be) spectroscopically identified with the Keck telescope are of magnitude $AB(8140) \approx 26$, of which there are another 200 or so that remain unidentified in the HDF. In time, spectroscopic redshift identifications of perhaps 300 objects—or roughly 10% of the total—might be obtained with the Keck telescope. What of the other 90%—the objects fainter than the spectroscopic limit?

Fortunately, it appears to be the case that broad-band photometric redshift techniques can be applied to accurately and reliably estimate redshifts of galaxies that are up to many magnitudes fainter than the spectroscopic limit. At low redshifts, the most prominent broad-band spectral feature is the 4000 Å spectral discontinuity, while at high redshifts the most prominent broad-band spectral feature is the Lyman spectral discontinuity, which is produced by intrinsic and intervening neutral hydrogen absorption. But the broad-band photometric redshift techniques make use not only of discrete spectral discontinuities but also of overall galaxy spectral energy distributions and so are applicable to galaxies that do not exhibit prominent broad-band spectral features (e.g. low-redshift, late-type galaxies) as well as to galaxies that do exhibit prominent broad-band spectral features (e.g. low-redshift, early-type galaxies or high-redshift galaxies). To magnitudes $AB(8140) \lesssim 26$, at which photometric redshifts can be compared with spectroscopic redshifts, the accuracy of the photometric redshifts is a few tenths and the reliability of the photometric redshifts approaches 100%. To even fainter magnitudes, at which numerical simulations can quantify the effects of photometric error, the accuracy and reliability of the photometric redshifts are plausibly sufficient to establish statistical moments of the galaxy distribution versus redshift, even to magnitudes close to the limiting magnitude thresholds of the images.

Interest in broad-band photometric redshift techniques has in the past been driven by the prospect of determining redshifts of galaxies at relatively low cost. Our interest is instead driven by the prospect of determining redshifts of galaxies that are inaccessible to ground-based spectroscopy at any cost, i.e. galaxies of very low luminosity or very high redshift. To bring this about, it is necessary first to make the case for the photometric redshifts. This is, of course, a difficult agenda, because the aim is to establish the validity of the photometric redshifts in a regime in which they by definition cannot be independently verified. Yet we believe this is also a crucially important agenda. The truly phenomenal progress toward observing normal galaxies at high redshifts made over the past several years has simultaneously revealed the possibilities and the limitations of ground-based spectroscopy with the Keck telescope. It is now clear that the very most luminous galaxies at redshifts $z \lesssim 4$ are accessible to Keck spectroscopy, but it is also now clear that lower-luminosity galaxies at redshifts much above $z \lesssim 4$ are probably not accessible to Keck spectroscopy. To push toward lower luminosities and higher redshifts it will almost certainly be necessary to rely on

broad-band photometric redshift techniques, perhaps supplemented by occasional spectra of very faint objects obtained with HST (which for faint, spatially unresolved objects at near-infrared and infrared wavelengths is a far more sensitive spectroscopic instrument than the Keck telescope).

The goal of this review is to make the case for the photometric redshifts. Happily, our task is made more manageable by recent progress on two fronts: First, at least six independent groups (besides ours) are estimating photometric redshifts of galaxies in the HDF—and are obtaining results that are in remarkable agreement with each other. (Comparisons of results of these independent analyses are presented by Ellis 1997 and Hogg et al. 1997.) Second, at least six independent groups are obtaining spectroscopic redshifts of galaxies in the HDF for comparison with the photometric redshifts. Although we concentrate on our own photometric analysis, much of what we report should apply to the various other photometric analyses, which are similar to our analysis in spirit if not in detail. We begin by briefly describing the technique in § 2 and the accuracy and reliability of the photometric redshifts in § 3. We continue by applying the broad-band photometric redshift technique to galaxies of redshift $z = 5 - 7$ in § 4 galaxies of redshift $z = 7 - 17$ in § 5 and to the redshift distribution of faint galaxies in § 6. We conclude by discussing possible future directions in § 7.

2. TECHNIQUE

2.1. Overview

Two conceptually different approaches have been applied to estimate photometric redshifts of galaxies in the HDF. The first technique, which we designate the “spectral template technique,” is to seek optimal agreement between the observed photometry and redshifted spectral templates. The spectral templates are constructed from observations of nearby galaxies or stellar population synthesis models and from observations of intervening neutral hydrogen absorption (measured by means of QSO absorption lines). The second technique, which we designate the “empirical technique,” is to seek optimal agreement between the observed photometry and polynomial fits to empirical correlations between fluxes, colors, and redshifts. The empirical correlations are established and calibrated with respect to known redshifts of spectroscopically identified galaxies. Practitioners of the two techniques are listed in Table 1.

The two techniques are subject to certain strengths and weaknesses as follows:

1. A strength of the spectral template technique is that it does not depend on the spectroscopic redshifts, whereas a weakness of the empirical technique is that it does depend on the spectroscopic redshifts. This is an issue because some fraction of the published spectroscopic redshifts are in error, and while the spectral template technique provides an independent check of the spectroscopic redshifts, the empirical technique can propagate errors in the spectroscopic redshifts into errors in the photometric redshifts.

2. A strength of the spectral template technique is that it can be applied to arbitrarily large redshifts, whereas a weakness of the empirical technique is that it cannot be applied to arbitrarily large redshifts.

3. A strength of the empirical technique is that it accounts for evolution of galaxy spectra with redshift, whereas a weakness of the spectral template technique is that it does not account for evolution of galaxy spectra with redshift (although the analysis of Gwyn & Hartwick 1996 does attempt to model time-evolving spectral templates).

Despite the difference inherent in the techniques, there seems to be general consensus that both techniques, properly applied, yield similar results over the common redshift interval at which they can be compared (cf. Ellis 1997; Hogg et al. 1997).

In the following sections, we describe our implementation of the spectral template technique, which is described in more detail by Lanzetta, Yahil, & Fernández-Soto (1996), Lanzetta, Fernández-Soto, & Yahil (1997), and Fernández-Soto, Lanzetta, & Yahil (1997, in preparation). Specifically, we describe our methods of (1) photometry and (2) redshift estimation, which are in principle the only aspects of the analysis upon which results of the broad-band photometric redshift techniques can depend.

2.2. Photometry

Our current analysis is based on the Version 2 optical images obtained by HST in December, 1995 using the Wide Field Planetary Camera 2 (WFPC2) and the F300W, F450W, F606W, and F814W filters (Williams et al. 1996) and on the Version 1 infrared images obtained by the Kitt Peak National Observatory (KPNO) 4 m telescope in April, 1996 using the IRIM camera and standard *J*, *H*, and *K* filters (Dickinson et al. 1997, in preparation). First, we identify objects in the F814W image using the SExtract source extraction program (Bertin & Arnouts 1996). Next, we measure the noise characteristics of the images by calculating empirical covariances, excluding pixels associated with identified objects. Next, we use non-overlapping isophotal aperture masks determined by the SExtract program to measure fluxes and flux uncertainties, applying different methods in the optical and infrared images.

To measure fluxes and flux uncertainties in the optical images, which are characterized by point spread functions of $\text{FWHM} \approx 0.1$ arcsec, we directly integrate within the aperture mask of every object detected in the F814W image. To measure fluxes and flux uncertainties in the infrared images, which are characterized by point spread functions of $\text{FWHM} \approx 1$ arcsec, we (1) model the spatial profile of every object detected in the F814W image as a convolution of the portion of the F814W image containing the object with the appropriate point spread function of the infrared image and (2) determine a least-squares fit of a linear sum of the model spatial profiles to the infrared image. The advantages of this method over simple aperture photometry are that (1) the flux measurements correctly weight signal-to-noise ratio variations within the spatial profiles and

(2) the flux uncertainty measurements correctly include the contributions of nearby, overlapping neighbors. The observed and modeled K -band images are shown in Figure 1.

Our analysis of the infrared images yields essentially optimal photometry under the assumption that the spatial profiles of the objects are independent of wavelength at observed-frame wavelengths $\lambda > 8140 \text{ \AA}$. This assumption may be justified as follows: At low redshifts, the infrared images measure rest-frame optical and infrared wavelengths, at which galaxy spatial profiles are observed to be more or less independent of wavelength. At high redshifts, galaxies are (as it turns out) physically small and unresolved by the infrared images at any wavelength. A similar analysis of deep ground-based optical images of the HDF (e.g. through medium-band filters) could certainly be applied to great advantage, making use of the unprecedented depth and spatial resolution of the F814W image to provide nearly ideal photometric spatial templates.

2.3. Redshift Estimation

First, we construct spectral templates of E/S0, Sbc, Scd, and Irr galaxies, including the effects of intrinsic and intervening neutral hydrogen absorption. Next, we integrate the redshifted spectral templates with the throughputs of the F300W, F450W, F606W, F814W, J , H , and K filters, at redshifts spanning $z = 0 - 7$. Next, we construct the “redshift likelihood function” of every object detected in the F814W image by calculating the relative likelihood of obtaining the measured fluxes and uncertainties given the modeled fluxes at an assumed redshift, maximizing with respect to galaxy spectral type and arbitrary flux normalization. Finally, we determine the maximum-likelihood redshift estimate of every object detected in the F814W image by maximizing the redshift likelihood function with respect to redshift.

The spectral templates are constructed from different sources at far-ultraviolet, near-ultraviolet and optical, and infrared wavelengths. First, we adopt empirical spectra of Coleman, Wu, & Weedman (1980) at wavelengths $\lambda = 1400 - 10,000 \text{ \AA}$. Next, we add spectra derived from simple power-law relationships motivated by results of Kinney et al. (1993) at wavelengths $\lambda = 912 - 1400 \text{ \AA}$. Next, we add spectra derived from stellar population synthesis models of Bruzual & Charlot (1993) at wavelengths $\lambda = 10,000 - 25,000 \text{ \AA}$. Finally, we include the effects intrinsic and intervening neutral hydrogen absorption (as a function of redshift) by (1) assuming that galaxies are optically thick at wavelengths shortward of the Lyman limit and (2) adding absorption from intervening Ly α -forest Ly α and Ly β absorption lines according to the “flux decrement” parameters D_A and D_B , measured by means of QSO absorption lines by Madau (1995) and Webb (1996, unpublished). The spectral templates are shown in Figure 2.

We experimented with spectral templates based at near-ultraviolet and optical wavelengths on (1) empirical spectra of Kinney et al. (1996) and (2) spectra derived from stellar population synthesis models of Bruzual & Charlot (1993). We abandoned these alternate spectral templates in favor of the adopted spectral templates because photometric redshifts determined with the alternate

spectral templates did not compare as favorably with the spectroscopic redshifts as photometric redshifts determined with the adopted spectral templates.

3. ACCURACY AND RELIABILITY OF PHOTOMETRIC REDSHIFTS

In this section we assess the accuracy and reliability of the photometric redshifts by (1) direct comparison of photometric and spectroscopic redshifts and (2) numerical simulations of the effects of photometric error on the photometric redshifts.

3.1. Photometric Redshifts: Successes and Failures

In preparation for the Hubble Deep Field Symposium, we set out in early May, 1997 to compare the available photometric redshifts with the available spectroscopic redshifts, which at the time numbered roughly 80 redshifts obtained with the Keck telescope. To our dismay, we found that a surprisingly large fraction (roughly 15%) of the photometric redshifts were clearly discordant with the spectroscopic redshifts, by amounts that were far too large to be attributed to photometric error. Believing that at the relatively bright magnitudes of the spectroscopic limit the reliability of the photometric redshifts should in principle be much higher than suggested by this comparison, we examined each of the discordant redshift pairs in detail, expecting to learn what caused the photometric redshifts to fail. Instead we found that in nearly every case it was the spectroscopic redshift—not the photometric redshift—that was in error.

That some fraction of the published spectroscopic redshifts are in error is hardly unexpected. After all, determining redshifts of extremely faint galaxies by any means—photometric or spectroscopic—is a difficult process subject to a variety of systematic uncertainties. But an uncritical acceptance of the validity of the spectroscopic redshifts has led some previous authors to incorrectly (and negatively) assess the reliability of the photometric redshifts. For this reason, it is important that any comparison of the photometric and spectroscopic redshifts begin by establishing under what circumstances both the photometric redshifts and the spectroscopic redshifts fail to yield reliable results. Our comparison of the photometric and spectroscopic redshifts in early May, 1997 identified eight spectroscopic redshifts that are ambiguous or in error and three photometric redshifts that are in error. (In two cases, both the spectroscopic and the photometric redshift are in error.) Here we describe each of the discordant cases, identifying galaxies by the Version 2 x and y mosaic pixel coordinates.

3.1.1. *The Successes*

Galaxy 1591,3681: This galaxy was assigned a spectroscopic redshift of $z = 0.13$ by Cowie

(1997) and a photometric redshift of $z = 1.20$ by our analysis. The galaxy occurs within ≈ 1 arcsec of a slightly brighter galaxy with no available spectroscopic redshift and a photometric redshift of $z = 0.16$. Considering typical ground-based seeing, it is likely that the spectroscopic redshift refers to the nearby galaxy, of which the photometric redshift is in excellent agreement with the spectroscopic redshift. In this case, the spectroscopic redshift is ambiguous or in error due to confusion with an overlapping source.

Object 2449,1574: This galaxy was assigned a spectroscopic redshift of $z = 0.318$ by Cowie (1997) and a photometric redshift of $z = 4.48$ by our analysis. The object occurs within ≈ 2 arcsec of a much brighter galaxy with a spectroscopic redshift of $z = 0.321$ and a photometric redshift of $z = 0.24$. The published spectra of the two objects are virtually identical although the colors of the two galaxies are very dissimilar, suggesting that one or the other or both of the spectra are incorrectly assigned. Subsequent spectroscopic observations of this object have established that it is a star (Cowie 1997, private communication). In this case, the spectroscopic redshift is in error due to operator error. This object is also noted below as a failure, because the photometric redshift is discordant with the actual redshift.

Galaxy 561,305: This galaxy was assigned a spectroscopic redshift of $z = 0.47$ by Cowie (1997) and a photometric redshift of $z = 0.76$ by our analysis. The galaxy occurs within ≈ 1 arcsec of a slightly brighter galaxy with no available spectroscopic redshift and a photometric redshift of $z = 0.48$. As in the case of galaxy 1591,3681, it is likely that the spectroscopic redshift refers to the nearby galaxy, of which the photometric redshift is in excellent agreement with the spectroscopic redshift. In this case, the spectroscopic redshift is ambiguous or in error due to confusion with an overlapping source.

Galaxies 790,1877 and 745,1845: These galaxies were assigned spectroscopic redshifts of $z = 0.511$ (Cowie 1997) and photometric redshifts of $z = 2.20$ (galaxy 790,1877) and $z = 0.56$ (galaxy 745,1845). The galaxies occur within ≈ 3 arcsec of each other. The published spectra of the two galaxies are identical, indicating that one or the other or both of the spectra are incorrectly assigned. In this case, the spectroscopic redshifts are ambiguous or in error due to operator error.

Galaxy 693,1224: This galaxy was assigned a spectroscopic redshift of $z = 1.231$ by Cowie (1997) and a photometric redshift of $z = 1.08$ by our analysis. The galaxy occurs within ≈ 1 arcsec of a galaxy with no available spectroscopic redshift and a photometric redshift of $z = 1.18$. As in the case of galaxy 1591,3681, it is likely that the spectroscopic redshift refers to the nearby galaxy, of which the photometric redshift is in excellent agreement with the spectroscopic redshift. In this case, the spectroscopic redshift is ambiguous or in error due to confusion with an overlapping source.

Galaxy 1816,1026: This galaxy was assigned a spectroscopic redshift of $z = 2.775$ by Steidel et al. (1996) and a photometric redshift of $z = 1.72$ by our analysis. The observed photometry of this galaxy is compared with the model spectrum of an Irr galaxy of redshift $z = 2.775$ in Figure 3. Results of Figure 3 indicate that the spectroscopic redshift cannot be correct unless our model of

intrinsic and intervening neutral hydrogen is grossly incorrect. Furthermore, our examination of the published spectrum of this galaxy (which is of moderate signal-to-noise ratio) fails to discern the claimed absorption features upon which the spectroscopic redshift is based. Subsequent analysis of the spectrum of this galaxy has failed to verify the spectroscopic redshift (Steidel 1997, private communication). In this case, the spectroscopic redshift is ambiguous or in error due to inaccurate identification of spectral features.

Galaxy 1193,3751: This galaxy was assigned a spectroscopic redshift of $z = 2.845$ by Steidel et al. (1996) and a photometric redshift of $z = 0.04$ by our analysis. The observed photometry of this galaxy is compared with the model spectrum of an Irr galaxy of redshift $z = 2.845$ in Figure 4. As in the case of galaxy 1816,1026, results of Figure 4 indicate that the spectroscopic redshift cannot be correct unless our model of intrinsic and intervening neutral hydrogen is grossly incorrect, and our examination of the published spectrum of this galaxy (which is of only moderate signal-to-noise ratio) fails to discern the claimed absorption features upon which the spectroscopic redshift is based. Subsequent spectroscopic observations of this galaxy have established a spectroscopic redshift of $z = 2.008$ (Steidel 1997, private communication). In this case, the spectroscopic redshift is in error due to inaccurate identification of spectral features. This galaxy is also noted below as a failure, because the photometric redshift is discordant with the actual redshift.

3.1.2. The Failures

Object 2449,1574: This object was assigned a photometric redshift of $z = 4.48$ by our analysis and a spectroscopic redshift of $z = 0.318$ by Cowie (1997), although as noted above subsequent spectroscopic observations of this object have established that it is a star (Cowie 1997, private communication). Our analysis does not include spectral templates of stars, which therefore must be removed by hand. In this case, the photometric redshift is in error due to confusion by a star.

Galaxy 1193,3751: This galaxy was assigned a photometric redshift of $z = 0.04$ by our analysis and a spectroscopic redshift of $z = 2.845$ by Steidel et al. (1996), although as noted above subsequent spectroscopic observations of this galaxy have established a spectroscopic redshift of $z = 2.008$ (Steidel 1997, private communication). The redshift likelihood function of this galaxy shows no local maxima near the actual redshift $z \approx 2.008$. In this case, the photometric redshift is in error due to cosmic variance with respect to the spectral templates. This galaxy is also noted above as a success, because the photometric analysis demonstrates that the original spectroscopic redshift cannot be correct.

Galaxy 3242,1972: This galaxy was assigned a photometric redshift of $z = 0.00$ by our analysis and a spectroscopic redshift of $z = 2.591$ by Steidel et al. (1996). The redshift likelihood function of this galaxy shows a local maximum at redshift $z = 2.00$, which has a likelihood 2.9σ less than the global maximum at $z = 0.00$. In this case, the photometric redshift is in error due to cosmic variance with respect to the spectral templates.

Galaxy 2888,1503: This galaxy was assigned a photometric redshift of $z = 1.32$ by our analysis and a spectroscopic redshift of $z = 2.268$ by Steidel et al. (1996). The redshift likelihood function of this galaxy shows no local maxima near the actual redshift $z \approx 2.268$. In this case, the photometric redshift is in error due to cosmic variance with respect to the spectral templates.

3.1.3. Summary

Spectroscopic redshifts of faint galaxies in the HDF are subject to a misidentification rate of $\approx 10\%$, which results from operator error, confusion with overlapping sources, and inaccurate identification of spectral features. Photometric redshifts of faint galaxies in the HDF are subject to a misidentification rate of $\approx 5\%$, which results from cosmic variance with respect to the spectral templates and confusion with stars.

3.2. Comparison of Photometric and Spectroscopic Redshifts

Spectroscopic redshift identifications of nearly 120 objects have been obtained with the Keck telescope as of August, 1997. Magnitudes of the spectroscopically identified objects range from $AB(8140) \approx 18$ through $AB(8140) \approx 26$, and redshifts of the spectroscopically identified objects range from $z \approx 0$ through $z \approx 4$. Excluding from consideration (1) spectroscopic redshifts that are described as ambiguous or in error in § 3.1.1 or as uncertain by the spectroscopic observers and (2) spectroscopic redshifts of stars (for which our analysis does not include spectral templates), spectroscopic redshifts of 102 galaxies are available for comparison with the photometric redshifts. Sources of the spectroscopic redshifts are listed in Table 3, and the comparison of photometric and spectroscopic redshifts is shown in Figure 5. Results of Figure 5 indicate that the photometric redshifts are in broad agreement with the spectroscopic redshifts. At redshifts $z < 2$, the photometric redshifts generally trace the spectroscopic redshifts, with no examples of photometric redshifts that are clearly discordant with the spectroscopic redshifts. At redshifts $z > 2$, the photometric redshifts generally trace the spectroscopic redshifts, with two examples of photometric redshifts that are clearly discordant with the spectroscopic redshifts. (The discordant redshifts arise from galaxies 1193,3751 and 3242,1972, which are discussed in § 3.1.2. In both cases, a high-redshift galaxy is incorrectly assigned a low redshift.)

To quantitatively assess the accuracy and reliability of the photometric redshifts by direct comparison of the photometric and spectroscopic redshifts, it is necessary to adopt some robust measure of the distribution of residuals between the photometric and spectroscopic redshifts. This is because (1) the residuals are not drawn from a Gaussian distribution and (2) the RMS residual is dominated by a few highly discordant redshifts, as is evident from Figure 5. Here we consider two such measures of the residuals: First, we consider the median absolute residual between the photometric and spectroscopic redshifts. Next, we consider the “clipped” RMS residual between

the photometric and spectroscopic redshifts. The clipped RMS residual is obtained by applying an iterative “sigma-clipping” algorithm to the residuals, rejecting as discordant photometric redshifts for which the residual exceeds three times the clipped RMS residual. According to this procedure, the “accuracy” of the photometric redshifts is measured by the clipped RMS residual and the “reliability” of the photometric redshifts is measured by the discordant fraction. Results are summarized in Table 3, which lists the sample condition, the median absolute residual, the clipped RMS residual, the number of discordant redshifts, the number of total redshifts, and the discordant fraction.

Several conclusions can be drawn from results of Table 3:

1. At the redshifts $z \approx 0 - 4$ spanned by the comparison of photometric and spectroscopic redshifts, the accuracy of the photometric redshifts is a few tenths and the reliability of the photometric redshifts approaches 100%. Specifically, the median absolute residual is 0.09, the clipped RMS residual is 0.17, and the discordant fraction is 0.049.

2. The accuracy of the photometric redshifts is greater at low redshifts than at high redshifts, but the *fractional* accuracy of the photometric redshifts is greater at high redshifts than at low redshifts. At redshifts $z < 2$, the clipped RMS residual is 0.09, which at a representative redshift $z = 0.5$ corresponds to a fractional accuracy of $\approx 18\%$. At redshifts $z > 2$, the clipped RMS residual is 0.40, which at a representative redshift $z = 3$ corresponds to a fractional accuracy of $\approx 13\%$.

3. The accuracy of the photometric redshifts is greater for late-type galaxies (which do not exhibit prominent broad-band spectral features) than for early-type galaxies (which do exhibit prominent broad-band spectral features). At redshifts $z < 2$ (at which early-type galaxies are found), the clipped RMS residual for late-type galaxies is 0.09 and the clipped RMS residual for early-type galaxies is 0.25.

There is some evidence that the photometric redshifts of galaxies at redshifts $z \gtrsim 2$ are systematically underestimated by ≈ 0.3 , especially at redshifts $z = 2 - 3$. If this systematic offset is accounted for, at redshifts $z > 2$ the clipped RMS residual is decreased to 0.24 and the discordant fraction is increased to 0.115. We have tried but failed to determine the cause of this systematic offset.

3.3. Photometric Error versus Cosmic Variance

There are in principle two effects that contribute to residuals between the photometric and spectroscopic redshifts: photometric error and cosmic variance with respect to the spectral templates. Here we evaluate the relative importance of photometric error and cosmic variance by means of a numerical simulation of the effect of photometric error on the photometric redshifts. First, we add random noise (according to the actual flux uncertainties) to the best-fit model fluxes of

every object detected in the F814W image. Next, we redetermine the maximum-likelihood redshift estimate of every object detected in the F814W image, using the simulated rather than measured fluxes. Finally, we repeat these steps 100 times in order to determine distributions of residuals between the actual and simulated redshifts. Results are summarized in Figure 6, which shows the distributions of residuals and the median absolute residuals between the actual and simulated redshifts as functions of magnitude and redshift.

Several conclusions can be drawn from results of Figure 6:

1. Photometric error produces almost no effect on the photometric redshifts at magnitudes $AB(8140) < 25$. At these magnitudes, the median absolute residual is no greater than 0.04, and the distributions of residuals are concentrated into single peaks centered at zero residual.

2. Photometric error produces a mild effect on the photometric redshifts at magnitudes $AB(8140) = 25 - 26$, which is somewhat more pronounced at redshifts $z > 2$ than at redshifts $z < 2$. Although at these magnitudes the median absolute residual (at all redshifts) is only 0.04 (which is comparable to the median absolute residual at brighter magnitudes), the distributions of residuals at high-redshifts are spread into small secondary peaks centered at large negative residuals in addition to prominent primary peaks centered at zero residual. These secondary peaks—which result from high-redshift galaxies that are incorrectly assigned low redshifts—contain 2.5% of the total at redshifts $z = 2 - 3$ and 6.1% of the total at redshifts $z = 3 - 4$.

3. Photometric error produces an increasingly significant effect on the photometric redshifts with increasing magnitude at magnitudes $AB(8140) > 26$. At redshifts $z = 0 - 1$, the effect of photometric error at faint magnitudes is to (1) increase the median absolute residuals and (2) produce long tails stretching to large positive residuals on the distributions of residuals. At redshifts $z > 1$, the effect of photometric error at faint magnitudes is to (1) increase the median absolute residuals and (2) produce prominent secondary peaks centered at large negative residuals on the distributions of residuals. At magnitudes $AB(8140) = 26 - 27$, these secondary peaks—which again result from high-redshift galaxies that are incorrectly assigned low redshifts—contain 9.7% of the total at redshifts $z = 2 - 3$ and 19.6% of the total at redshifts $z = 3 - 4$.

4. At faint magnitudes, it is more likely that high-redshift galaxies will be incorrectly assigned low redshifts than that low-redshift galaxies will be incorrectly assigned high redshifts. For example, at magnitudes $AB(8140) = 27 - 28$, the long tail stretching to large positive residuals at redshifts $z = 0 - 1$ contains 27.3% of the total while the secondary peak at large negative residuals at redshifts $z = 3 - 4$ contains 34.8% of the total.

It is possible to draw general conclusions about the relative importance of photometric error and cosmic variance on the photometric redshifts by combining results of Figure 6 with results of § 3.2. At redshifts $z < 2$, magnitudes of the spectroscopically identified objects range from $AB(8140) = 18.16$ through $AB(8140) = 24.88$, with a median of $AB(8140) = 22.68$. Results of Figure 6 indicate that at these magnitudes photometric error produces almost no effect on the photometric redshifts. At redshifts $z > 2$, magnitudes of the spectroscopically identified objects

range from $AB(8140) = 23.40$ through $AB(8140) = 26.75$ with a median of $AB(8140) = 25.08$. Results of Figure 6 indicate that at these magnitudes photometric error produces at most a mild effect on the photometric redshifts. [For example, even at magnitudes as faint as $AB(8140) = 26 - 27$, the median absolute residual produced by cosmic variance is less than the median absolute residual between the photometric and spectroscopic redshifts, although the discordant fraction produced by cosmic variance is consistent with the discordant fraction between the photometric and spectroscopic redshifts.] We therefore conclude that *residuals between the photometric and spectroscopic redshifts are dominated by cosmic variance rather than by photometric error*.

This result establishes the magnitude of the effect of cosmic variance on the photometric redshifts. Specifically, by attributing the entire residual between the photometric and spectroscopic redshifts to the effect of cosmic variance and considering the redshifts $z \approx 0 - 4$ spanned by the comparison of photometric and spectroscopic redshifts, we conclude that cosmic variance produces a median absolute residual of 0.09, a clipped RMS residual of 0.17, and a discordant fraction of 0.049. As long as the effect of cosmic variance does not increase with decreasing galaxy luminosity—and we can think of no reason that it should—then *these values must apply at all magnitudes*, not just the relatively bright magnitudes of the spectroscopic limit. In practice, this has two important implications: First, at magnitudes brighter than $AB(8140) \approx 26 - 27$ the accuracy and reliability of the photometric redshifts is limited by cosmic variance and at magnitudes fainter than $AB(8140) \approx 26 - 27$ the accuracy and reliability of the photometric redshifts is limited by photometric error. Second, the uncertainty associated with any statistical moment of the galaxy distribution—including the effects of sampling error, photometric error, and cosmic variance—may be realistically estimated by means of a “bootstrap” resampling technique, simulating the effect of photometric error by adding random noise to the fluxes and simulating the effect of cosmic variance by adding (rather modest) random noise to the estimated redshifts. We expect that this technique will ultimately play an important role in exploiting the full potential of the broad-band photometric redshift techniques.

4. GALAXIES OF REDSHIFT $z = 5 - 7$

In this section we describe an application of the broad-band photometric redshift techniques to galaxies of redshift $z = 5 - 7$. A full description of this analysis is reported by Lanzetta, Fernández-Soto, & Yahil (1997).

Results of § 3 demonstrate the accuracy and reliability of the broad-band photometric redshift techniques at the redshifts $z \approx 0 - 4$ spanned by the comparison of photometric and spectroscopic redshifts. But our analysis identifies galaxies with estimated redshifts as large as $z \approx 5 - 7$, which are probably inaccessible to ground-based spectroscopy. These galaxies are characterized by strong flux at observed-frame wavelengths $\lambda \approx 8140 \text{ \AA}$ and an absence of detectable flux at shorter wavelengths, hence it is not possible by means of optical observations alone to establish continuum spectral energy distributions of the galaxies or to definitively rule out the competing alternatives

that (1) the flux detected at observed-frame wavelengths $\lambda \approx 8140 \text{ \AA}$ arises due to strong emission lines or (2) the absence of detectable flux at shorter wavelengths arises due to reddening by dust.

To address these issues, we consider the infrared images obtained with the KPNO 4 m telescope by Dickinson et al. (1997, in preparation). Specifically, we concentrate on galaxy 2342,968, which is the brightest galaxy with estimated redshift $z > 5$ (at least at 8140 \AA). The infrared photometric analysis applied to galaxy 2342,968 is shown in Figure 7, and the spectral energy distribution of galaxy 2342,968 is shown in Figure 8. Results of Figures 7 and 8 indicate that galaxy 2342,968 is detected at the 0.9σ level of significance at the J band, the 2.7σ level of significance at the H band, and the 4.7σ level of significance at the K band. The primary conclusions of the analysis are two-fold: First, the detection of galaxy 2342,968 at the J , H , and K infrared bands establishes the continuum spectral energy distribution at observed-frame wavelengths spanning $\lambda \approx 8140 \text{ \AA}$ through $\lambda \approx 2.2 \mu$. This rules out the possibility that galaxy 2342,968 is a lower-redshift galaxy that exhibits a strong emission line at observed-frame wavelength $\lambda \approx 8140 \text{ \AA}$. Second, the detection of galaxy 2342,968 at modest flux levels at the J , H , and K infrared bands limits the permitted reddening. This rules out the possibility that galaxy 2342,968 is a lower-redshift galaxy that is heavily obscured and reddened by dust.

To establish a quantitative measure of the degree to which heavily obscured and reddened lower-redshift galaxies can be ruled out, we repeat the maximum-likelihood redshift determinations of our previous analysis, modifying the galaxy spectral templates by a grid of dust extinction models with color excess $E(B-V)$ ranging from $E(B-V) = 0$ (no dust obscuration) through $E(B-V) = 4$ (very heavy dust obscuration). It is possible to find acceptable high-redshift solutions with very modest amounts of dust extinction, but it is not possible to find acceptable low-redshift solutions with larger amounts of dust extinction. In particular, any solution with $z < 4.4$ is ruled out at more than the 4σ level of significance. The reason is that it is not possible to simultaneously satisfy the sharp discontinuity in flux between the F606W and F814W filters and the absence of strong infrared flux with any low-redshift galaxy spectral template and any amount of dust extinction. A similar analysis applied to the other galaxies with estimated redshift $z > 5$ yields similar results, although with less stringent limits. We conclude that the available evidence supports the photometric redshift identifications and that it is very unlikely that at least the brightest of the galaxies with estimated redshifts $z > 5$ are at substantially lower redshifts.

5. REDSHIFT DISTRIBUTION OF FAINT GALAXIES

Our analysis determines photometric redshifts of over 2500 galaxies, which together with an assessment of the effects of photometric error and cosmic variance can be used to construct an essentially exhaustive account of statistical properties (and uncertainties) of faint galaxies at magnitudes ranging to $AB(8140) \approx 30$ and redshifts ranging to $z \approx 7$. A complete enumeration of the properties of faint galaxies is beyond the scope of this review, so we instead illustrate the utility of broad-band photometric redshift techniques by presenting the redshift distribution of faint galaxies.

The redshift distribution and median redshift of faint galaxies as functions of limiting magnitude threshold are shown in Figure 9:

Several conclusions can be drawn from results of Figure 9:

1. At the brightest magnitudes $AB(8140) \approx 23$ accessible to the HDF, the galaxy redshift distribution is peaked at low redshifts with a median redshift of $z = 0.64$. This agrees with results of deep ground-based galaxy surveys, the deepest of which are sensitive to comparable magnitudes (e.g. Cowie et al. 1996).

2. High-redshift galaxies with $z > 2$ become prominent at magnitudes $AB(8140) \approx 25$, at which they constitute $\approx 6.1\%$ of the galaxy population. At fainter magnitudes, high-redshift galaxies become increasingly prominent with increasing magnitude threshold. Galaxies of redshift $z > 2$ constitute $\approx 13.9\%$ of the galaxy population at magnitudes $AB(8140) < 26$, 19.5% of the galaxy population at magnitudes $AB(8140) < 27$, and 24.0% of the galaxy population at magnitudes $AB(8140) < 28$.

4. The median redshift of the galaxy redshift distribution increases monotonically with increasing magnitude threshold. The median redshift of the galaxy redshift distribution grows from med $z = 0.68$ at magnitudes $AB(8140) < 24$, to med $z = 1.04$ at magnitudes $AB(8140) < 26$, to med $z = 1.36$ at magnitudes $AB(8140) < 28$.

5. The galaxy redshift distribution exhibits a precipitous decline at redshift $z \approx 2$ at all magnitudes $AB(8140) \gtrsim 26$. This is unlikely to be an artifact of the analysis because (1) results of § 3 indicate that redshifts $z > 2$ exhibit a comparable accuracy to redshifts $z < 2$ and (2) there are prominent broad-band spectral features redshifted into the optical filters at redshifts $z \approx 2$.

6. FUTURE DIRECTIONS

Our conclusion is that broad-band photometric redshift techniques can be applied to accurately and reliably estimate redshifts of galaxies that are inaccessible to ground-based spectroscopy. At bright magnitudes the reliability of the photometric redshifts compares favorably with the reliability of the spectroscopic redshifts, and at faint magnitudes the effects of photometric error on the photometric redshifts can be rigorously quantified and accounted for. Yet we suspect that the ability of broad-band photometric techniques to reliably identify galaxies at redshifts beyond the ground-based spectroscopic limit will not become generally accepted until some means of independent verification can be found. The very brightest galaxy at estimated redshifts $z > 5$ (galaxy 2342,968) is of magnitude $AB(8140) = 26.3$, which is probably inaccessible to Keck spectroscopy. How, then, is progress to be made?

It is easy to show that for background-limited observations of spatially unresolved objects, the ratio of exposure times needed to obtain a given signal-to-noise ratio for space-based versus

ground-based observations (assuming identical system throughputs and bandpasses) scales as

$$\frac{t_{\text{ground}}}{t_{\text{space}}} = \frac{f_{\nu}(\text{sky})_{\text{ground}}}{f_{\nu}(\text{sky})_{\text{space}}} \frac{A_{\text{space}}}{A_{\text{ground}}} \frac{\Omega(\text{sky})_{\text{ground}}}{\Omega(\text{sky})_{\text{space}}}, \quad (1)$$

where $f_{\nu}(\text{sky})$ is the sky brightness, A is the telescope aperture, and $\Omega(\text{sky})$ is the solid angle subtended by a spatial resolution element. At near-infrared wavelengths the first term of this expression evaluates to ≈ 4.4 , for HST versus the Keck telescope the second term evaluates to ≈ 0.06 , and for space-based seeing of ≈ 0.1 arcsec versus (optimistic) ground-based seeing of ≈ 0.6 the third term evaluates to ≈ 36 . Forming the product of these three terms, we conclude that *HST is roughly 10 times more sensitive than the Keck telescope for spectroscopy of faint, spatially unresolved objects*. Although the Keck telescope can take advantage of multi-object spectroscopic capabilities—which HST with STIS probably cannot—this is not an issue for objects at the very limit of detectability or for objects of very low spatial density. We believe that to establish the broad-band photometric techniques at magnitudes and redshifts beyond the spectroscopic limit it will be necessary to use HST with STIS obtain spectroscopic confirmation of a few targets chosen carefully on the basis of broad-band photometric redshifts. These observations will provide the means of establishing the effects of cosmic variance on the photometric redshifts at redshifts $z \gtrsim 4$.

We are grateful to R. Williams and the staff of STScI for providing access to the reduced optical images, to M. Dickinson for providing access to the reduced infrared images, and to C. Steidel and M. Dickinson providing access to spectroscopic redshifts in advance of publication. A.F.-S. and K.M.L. were supported by NASA grant NAGW-4422 and NSF grant AST-9624216.

TABLE 1
 PRACTITIONERS OF BROAD-BAND
 PHOTOMETRIC REDSHIFT TECHNIQUES

Group	Technique	Reference
Hawaii	spectral template	1
Imperial College	spectral template	2
Johns Hopkins	empirical	3
Stony Brook	spectral template	4
Toronto	spectral template	5
Victoria	spectral template	6

REFERENCES—(1) Cowie 1997; (2) Mobasher et al. 1996; (3) Connolly et al. 1997; (4) Lanzetta, Yahil, & Fernández-Soto 1996; (5) Sawicki et al. 1997; (6) Gwyn & Hartwick 1996.

TABLE 2
SOURCES OF SPECTROSCOPIC
REDSHIFTS

Group	Reference
Berkeley	1
Caltech	2
Elston	3
Hawaii	4
Lick	5
Steidel et al.	6,7

REFERENCES—(1) Zepf, Moustakas, & Davis 1997; (2) Cohen et al. 1997; (3) Elston 1997, private communication; (4) Cowie 1997; (5) Lowenthal et al. 1997; (6) Steidel et al. 1996; (7) Dickinson et al. 1997, this volume.

TABLE 3
COMPARISON OF PHOTOMETRIC AND SPECTROSCOPIC REDSHIFTS

Condition	Median	Clipped RMS			
	Absolute	Residual	Discordant	Total	Discordant
	Residual		Number	Number	Fraction
All	0.09	0.17	5	102	0.049
$z < 2$	0.08	0.09	4	78	0.051
$z > 2$	0.32	0.40	2	24	0.083
$z < 2$, “early type”	0.12	0.25	0	10	0.000
$z < 2$, “late type”	0.07	0.09	2	68	0.029

REFERENCES

- Bertin, E. & Arnouts, S. 1996, A&AS, in press
- Bruzual, G., & Charlot, S. 1993, ApJ, 378, 47
- Cohen, J. G., Cowie, L. L., Hogg, D. W., Songaila, A., Blandford, R., Hu, E. M., & Shopbell, P. 1996, ApJ, 471, L5
- Coleman, G. D., Wu, C. C. & Weedman, D. W. 1980, ApJS, 43, 393
- Connolly, A. J., Szalay, A. S., Dickinson, M., Subbarao, M. U., Brunner, R. J. 1997, ApJ, 486, L11
- Cowie, L. L. 1997, <http://www.ifa.hawaii.edu/~cowie/tts/tts.html>
- Cowie, L. L., Songaila, A., Hu, E. M., & Cohen, J. G. 1996, AJ, 112, 839
- Ellis, R. S. 1997, ARAA, in press
- Gwyn, S. D. J., & Hartwick, F. D. A. 1996, ApJ, 468, L77
- Hogg, D. W., Cohen, J. G., Blandford, R., Gwyn, S. D. J., Hartwick, F. D. A., Mobasher, B., Mazzei, P., Sawicki, M., Lin, H., Yee, H. K. C., Connolly, A. J., Brunner, R. J., Csabai, I., Dickinson, M., Subbarao, M. U., Szalay, A. S., Fernández-Soto, A., Lanzetta, K. M., & Yahil, A. 1997, AJ, submitted
- Kinney, A. L., Bohlin, R. C., Calzetti, D., Panagia, N. & Wyse, R. F. G. 1993, ApJS, 86, 5
- Lanzetta, K. M., Fernández-Soto, A., & Yahil, A. 1997, ApJ, submitted
- Lanzetta, K. M., Yahil, A., & Fernández-Soto, A. 1996, Nature, 381, 759
- Lowenthal, J. D., Koo, D. C., Guzmán, R., Gallego, J., Phillips, A. C., Faber, S. M., Vogt, N. P., Illingworth, G. D., & Gronwall, C. 1997, ApJ, 481, 673
- Madau, P. 1995, ApJ, 441, 18
- Mobasher, B., Rowan-Robinson, M., Georgakakis, A., Eaton, N. 1996, MNRAS, 282, L7
- Sawicki, M. J., Lin, H., & Yee, H. K. C. 1997, AJ, 113, 1
- Steidel, C. C., Giavalisco, M., Dickinson, M., & Adelberger, K. 1996, AJ, 112, 352
- Williams, R. E., et al. 1996, AJ, 112, 1335
- Zepf, S. E., Moustakas, L. A., & Davis, M. 1997, ApJ, 474, L1

Fig. 1.— Observed (left panel) and modeled (right panel) K -band images. Angular extent is $x.xx \times x.xx$ arcmin², and spatial resolution is FWHM ≈ 1 arcsec.

Fig. 2.— Spectral templates of E/S0 (solid curve), Sbc (dotted curve), Scd (short dashed curve), and Irr (long dashed curve) galaxies.

Fig. 3.— Observed photometry of galaxy 1816,1026 compared with model spectrum of an Irr galaxy of redshift $z = 2.775$. Vertical error bars indicate 1σ uncertainties and horizontal error bars indicate filter FWHM. It is very unlikely that the redshift of the galaxy is $z = 2.775$.

Fig. 4.— Observed photometry of galaxy 1193,3751 compared with model spectrum of an Irr galaxy of redshift $z = 2.845$. Vertical error bars indicate 1σ uncertainties and horizontal error bars indicate filter FWHM. It is very unlikely that the redshift of the galaxy is $z = 2.845$.

Fig. 5.— Comparison between photometric redshifts z_{phot} and spectroscopic redshifts z_{spec} . Solid line shows $z_{\text{phot}} = z_{\text{spec}}$.

Fig. 6.— Distributions of residuals between best-fit model and simulated redshifts, illustrating the effects of photometric error on the photometric redshifts. Panels are arranged horizontally according to magnitude, from $AB(8140) = 21 - 22$ through $AB(8140) = 29 - 30$ in steps of 1 mag, and vertically according to redshift, from $z = 0 - 1$ through $z = 4 - 5$ in steps of 1. The median absolute residual is listed at the upper right corner of every panel.

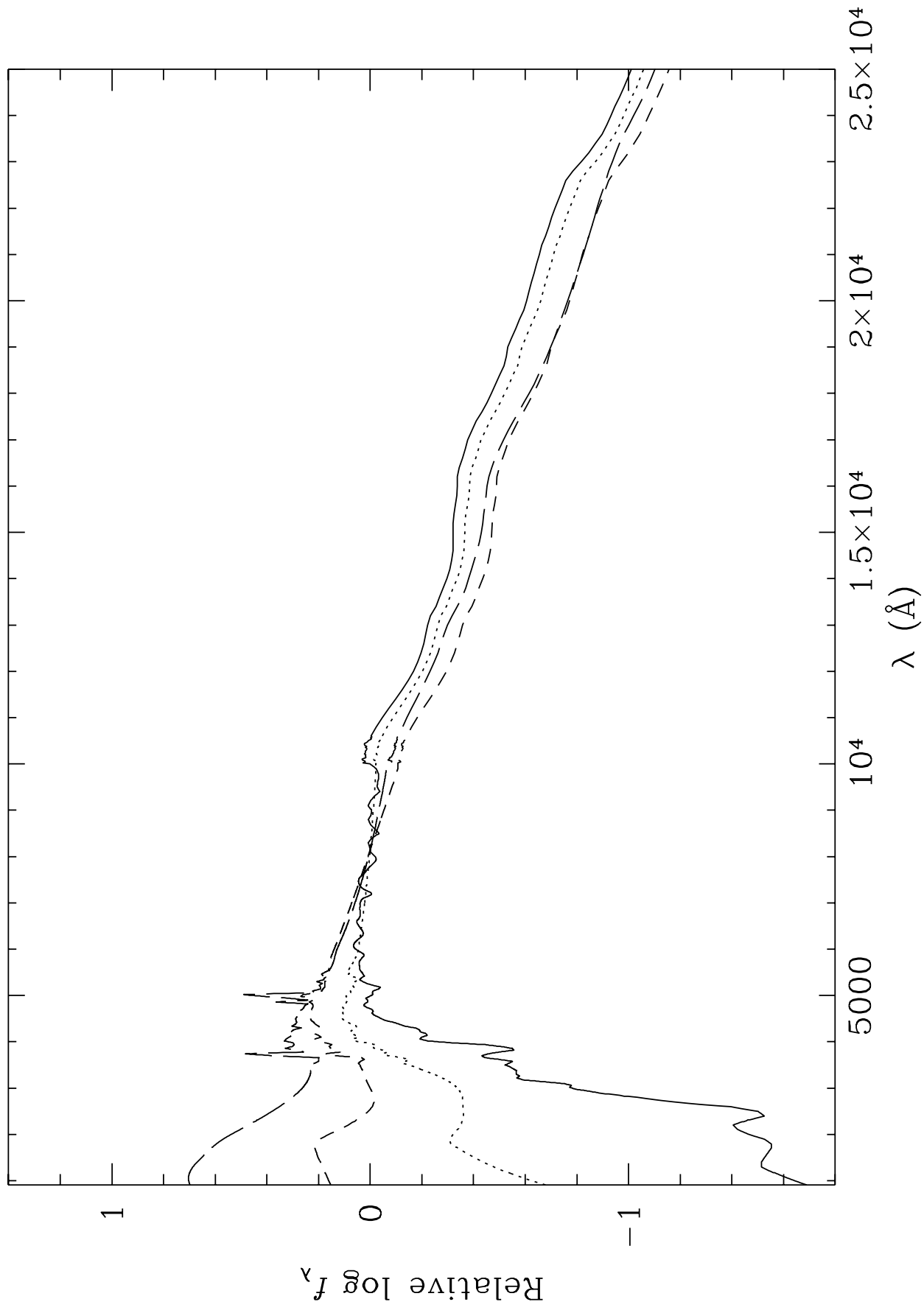
Fig. 7.— Infrared photometric analysis applied to galaxy 2342,968. Angular extent of each image is 20.5×20.5 arcsec². Left panels show J -band images, center panels show H -band images, and right panels show K -band images. Top panels show raw images, and bottom panels show images for which models of all objects other than galaxy B have been subtracted. Arrows point to the expected position of galaxy B, as measured from the F814W image.

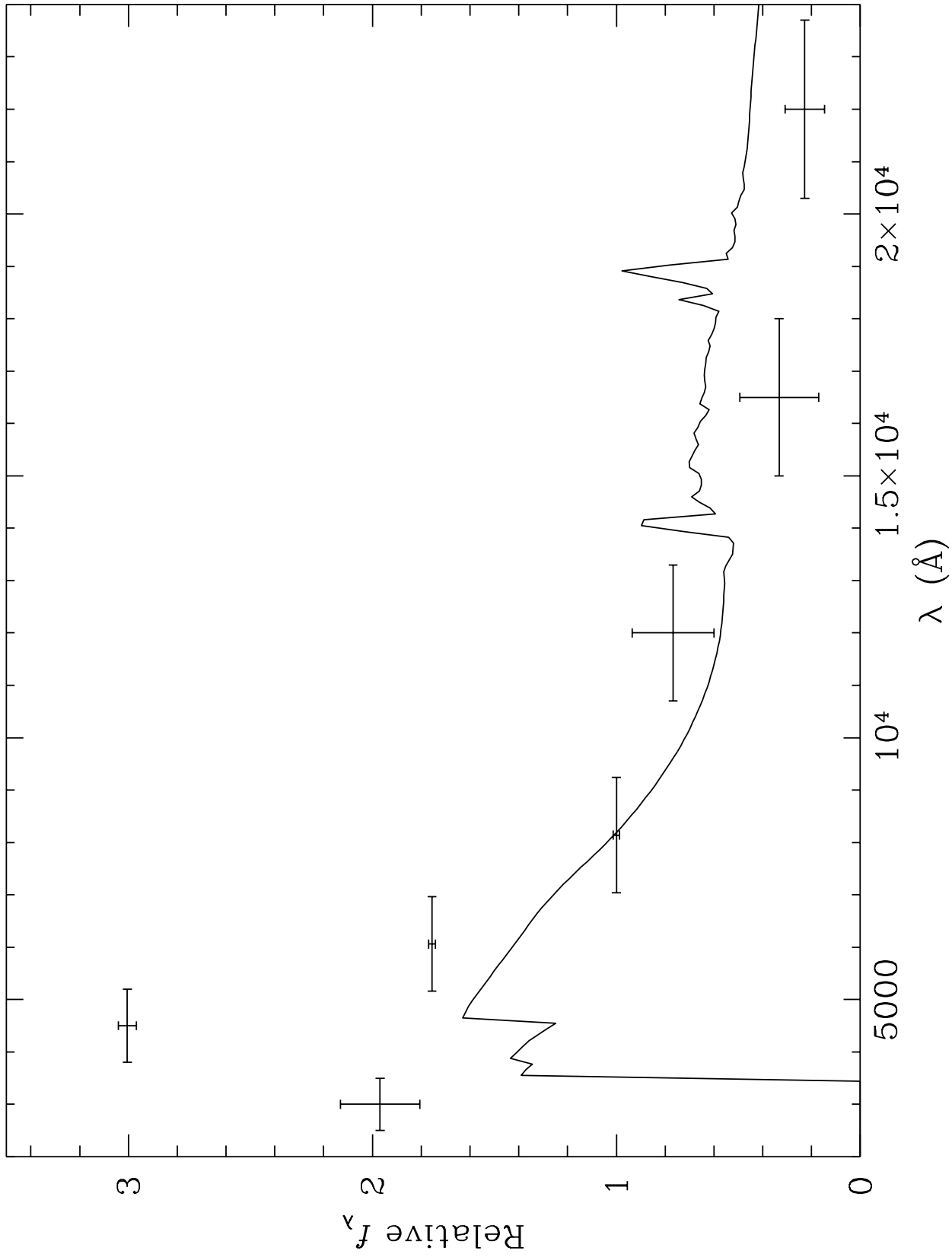
Fig. 8.— Spectral energy distribution of galaxy 2342,968. Vertical error bars indicate flux uncertainties, and horizontal error bars indicate filter FWHM.

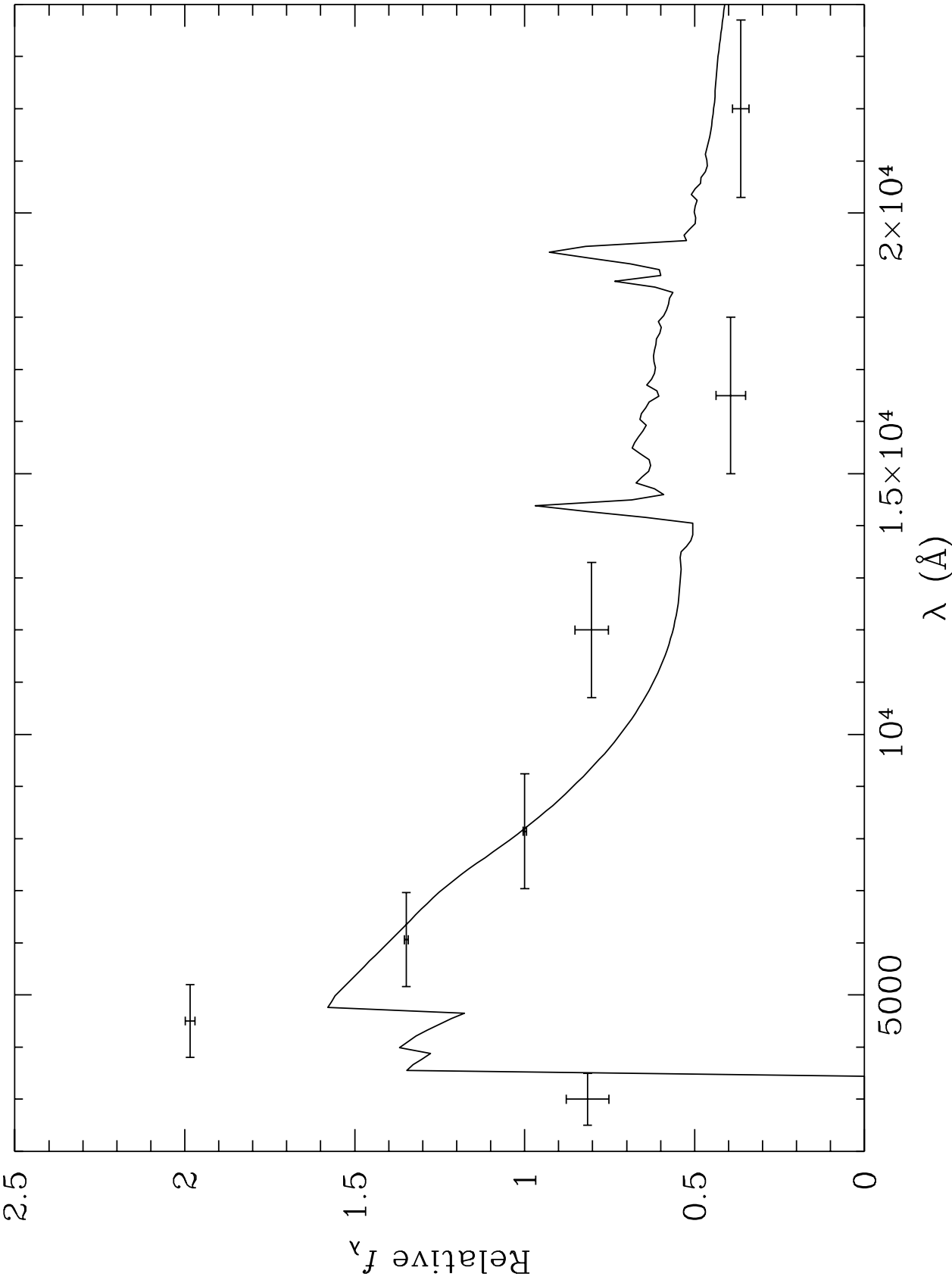
Fig. 9.— Redshift distribution of faint galaxies as a function of limiting magnitude threshold. The limiting magnitude threshold and median redshift is listed in every panel.

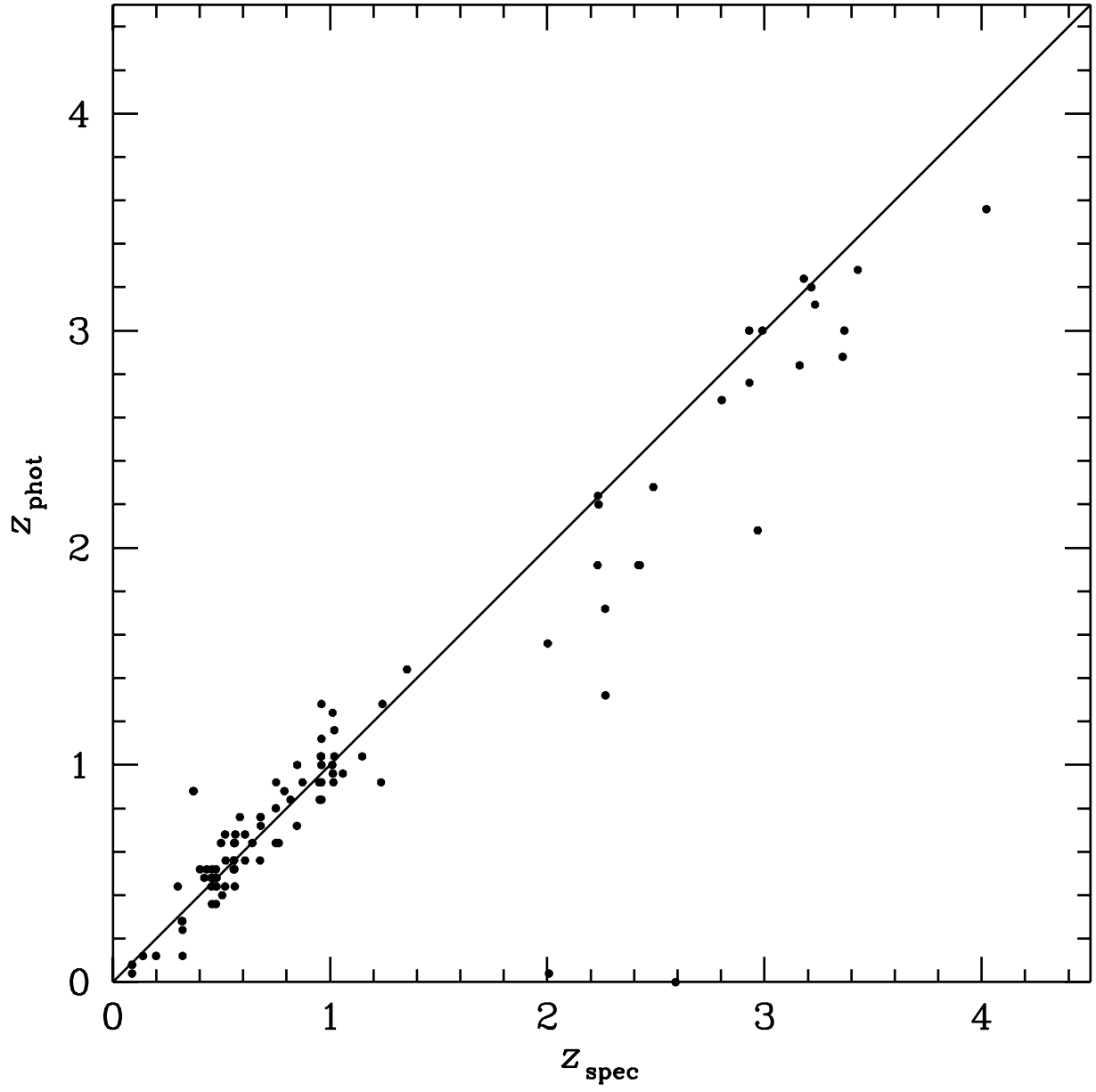
This figure "figure1.jpg" is available in "jpg" format from:

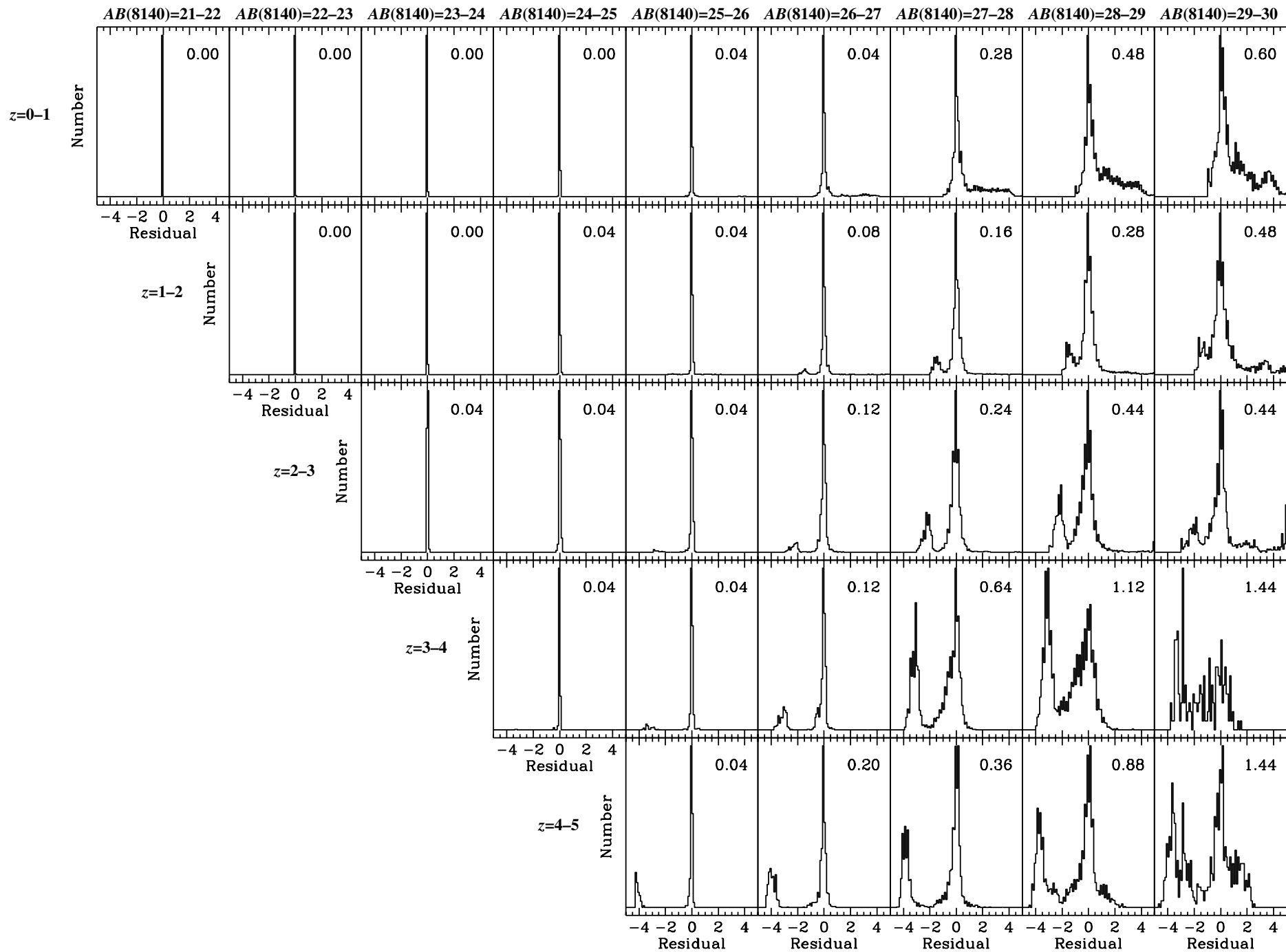
<http://arxiv.org/ps/astro-ph/9709166v1>











This figure "figure7.jpg" is available in "jpg" format from:

<http://arxiv.org/ps/astro-ph/9709166v1>

